

High-triplet-energy derivatives of indole and carbazole as hosts for blue phosphorescent organic light-emitting diodes

Dalius Gudeika¹, Karolis Norvaisa¹, Egle Stanislovaityte¹, Oleksandr Bezikonnyi¹, Dmytro Volyniuk¹, Pavlo Turyk¹, Iryna Hladka¹, Valeriy M. Yashchuk², Juozas V. Grazulevicius^{1*}

¹ Department of Polymer Chemistry and Technology, Kaunas University of Technology, Radvilenu Plentas 19, LT50254, Kaunas, Lithuania

² Taras Shevchenko National University of Kyiv, Kiev, Ukraine

* Corresponding author: Juozas.Grazulevicius@ktu.lt (Juozas V. Grazulevicius)

Abstract

The synthesis and characterization of a series of electro-active compounds containing carbazolyl and indolyl moieties are reported. All the synthesized derivatives were capable of glass formation with the glass transition temperatures ranging from 89 to 130 °C. They showed high thermal stability with the 5% weight loss temperatures ranging from 370 to 412 °C. The obtained compounds emit light in the deep blue region (350-366 nm) and their solutions exhibit moderately high fluorescence quantum yields in the range of 22.9-44.2%. The compounds exhibited high triplet-energy levels ranging from 2.70 to 3.06 eV. The solid-state ionization potentials of the synthesized compounds were found to be comparable (5.68 - 5.72 eV). They are characterized by equal values of the optical band gaps (3.53 eV). Cyclic voltammetry revealed two irreversible oxidation peaks with the onsets at 0.95 V and 1.35 V in the repeated cycles. 9-{4-[Bis(1-ethyl-2-phenyl-1*H*-indol-3-yl)methyl]phenyl}-9*H*-carbazole exhibited well balanced hole and electron mobilities reaching $1.3 \times 10^{-3} \text{ cm}^2/\text{V} \times \text{s}$ at electric fields higher than $8.1 \times 10^5 \text{ V/cm}$. The compounds

were tested as hosts in electrophosphorescent devices. The best device showed turn-on voltage of 2.4 V (at 1 cd/m²); maximum current efficiency of 44.7 cd/A, maximum brightness of 4500 cd/m² (at 7 V), maximum power efficiency of 38 lm/W, and external quantum efficiency of *ca.* 18 %.

Keywords: Cyclic voltammetry, triplet-energy level, host, hole and electron mobilities, external quantum efficiency.

1. Introduction

Phosphorescent organic light-emitting diodes (PhOLEDs) were developed as solid-state light sources for flexible flat big-area displays and highly-efficient solid-state lighting [1]. The great interest in PhOLEDs is based on their ability of harvesting of both singlet and triplet excitons for light emission [2]. Although the similar harvesting efficiency was recently discovered for the devices based on thermally activated delayed fluorescence (TADF) [3,4], PhOLEDs remain commercially attractive due to their high efficiency and stability. Since the first report on PhOLEDs [5], their output parameters such as external quantum efficiency, long-time stability, turn-on voltage, color purity *etc.* were well improved partly because of variety of the developed highly-effective charge-transporting materials which were utilized as the hosts or for additional layers [6,7,8]. The search for new materials with the improved physical parameters such as charge-carrier mobility (μ), triplet energy (T_1), glass-transition temperature (T_g) is still an urgent task. This is of particular importance in the case of blue PhOLEDs, which show inferior efficiency relative to those of green or red PhOLEDs [9]. High T_g is preferred for electroactive organic materials since higher T_g is generally related to higher morphological stability of amorphous films [10]. Since the first triplet energy levels for blue phosphorescent emitters are usually higher than *ca.* 2.7 eV, effective light-emitting layers can be obtained based if high-triplet-energy hosts are used. The usage of such hosts enables to reduce energy leakage through the triplets [11]. High energies needed to produce

blue electroluminescence rise the special requirements for the photostability of the materials used in
© 2018. This manuscript version is made available under the CC-BY-NC-ND 4.0 license
<http://creativecommons.org/licenses/by-nc-nd/4.0/>

blue PhOLEDs [12]. The efforts to develop efficient and reliable blue PhOLEDs are aggravated by the lack of efficient charge transporting materials with a wide energy gap for sufficient carrier injection [13]. Therefore, high triplet energy moieties such as carbazole or indole have to be utilized in the molecular design of high-triplet-energy hosts [6]. Carbazole and 1,3,4-oxadiazole based host materials having relatively high triplet energies (*ca.* 2.70 eV) and bipolar charge transport capabilities with the charge mobilities of 10^{-5} - 10^{-6} $\text{cm}^2 \times \text{V}^{-1} \times \text{s}^{-1}$ were reported to be suitable for the fabrication of blue, green, yellow, orange, red, and white PhOLEDs with high external quantum efficiencies (EQE) of *ca.* 20%. [14]. Indolo [3,2,1-jk]carbazole host materials with T_g exceeding 110 °C, and high triplet energies (> 2.81 eV) were utilized for blue and green PhOLEDs with EQE of *ca.* 15% [15]. Compounds containing carbazolyl and benzimidazolyl moieties ($T_1 > 2.9$ eV) were used as hosts in blue, green and orange PhOLEDs with EQE ranging from 22 to 27% [16]. The expedient selection of host materials can enable to obtain blues PhOLEDs with increased efficiency [17].

The aim of this work is synthesis of glass-forming high-triplet-energy derivatives of indole and carbazole as hosts for blue PhOLEDs and investigation of their thermal, optical, photophysical, electrochemical, photoelectrical properties. The most promising compounds were tested as hosts in the simple blue PhOLEDs using a commercially available phosphorescence emitter bis(4',6'-difluorophenylpyridinato)-iridium(III) picolate (FIrpic).

2. Experimental Section

2.1. Materials

5-Methoxyindole, 1-bromoethane, 2-phenylindole, tetra-n-butylammonium bromide, molybdenum trioxide (MoO_3), bis(4',6'-difluorophenylpyridinato)-iridium(III) picolate (FIrpic), 4,4',4''-tris[3-methylphenyl(phenyl)amino]triphenylamine (*m*-MTDATA), 2,2',2''-(1,3,5-

© 2018. This manuscript version is made available under the CC-BY-NC-ND 4.0 license
<http://creativecommons.org/licenses/by-nc-nd/4.0/>

benzinetriyl)-tris(1-phenyl-1-*H*-benzimidazole) (TPBi), *N,N'*-di(1-naphthyl)-*N,N'*-diphenyl-(1,1'-biphenyl)-4,4'-diamine (NPB) and 2,9-dimethyl-4,7-diphenyl-1,10-phenanthroline (BCP) were purchased from Sigma Aldrich and Fluka and used as received. The solvents were dried and distilled prior to use. 4-(9*H*-Carbazol-9-yl)benzaldehyde (**I**, m.p. 152-154 °C, lit. [18] m.p. 156.0-158.0 °C), 1-(4-methoxy-phenyl)-2-methyl-1*H*-indole (**III**) m.p. 69-71 °C, lit. [19] m.p. 69-71 °C were synthesized according to the reported procedures [18,19].

2.2. Instrumentation

NMR spectra were recorded using deuterated chloroform or dimethyl sulfoxide as solvents with Varian Unity Inova spectrometer operating at 300 MHz for ¹H and 75.4 MHz for ¹³C nuclei, respectively. All the data are given as chemical shifts δ (ppm) downfield from TMS. IR-spectra of the samples in KBr pellets were recorded on a Perkin Elmer Spectrum GX FT-IR system spectrometer. Mass (MS) spectra were obtained on a Waters ZQ 2000 (Milford, USA). Elemental analysis was performed with an Exeter Analytical CE-440 Elemental Analyser. Differential scanning calorimetry (DSC) measurements were performed on a Q2000 thermosystem at a heating/cooling rate of 10 °C min⁻¹ under nitrogen atmosphere. Melting points (m.p.) were recorded on Electrothermal MEL-TEMP melting point apparatus. Thermogravimetric (TG) analyses were executed on a TA Instruments Q50 under nitrogen atmosphere at a heating rate of 20 °C min⁻¹. Absorption spectra of dilute solutions were recorded by AvaSpecUSB2 spectrometer. Photoluminescence (PL) spectra of the materials were recorded using Edinburgh Instruments FLS980 fluorescence spectrometer. For recording the absorption and PL spectra, dilute solutions of the compounds were prepared by dissolving them in spectral grade tetrahydrofuran (THF) at 1×10⁻⁵ M concentration. Cyclic voltammetry measurements were performed on a μ -Autolab Type III potentiostat (EcoChemie, Netherlands). The data were collected using General Purpose

Electrochemical System (GPES) software. Electrochemical experiments were carried out at room temperature using a three-electrode cell consisting of a glassy carbon working electrode, a platinum coil as counter electrode and a silver wire as reference electrode. 0.1 M solution of *n*-Bu₄NPF₆ in dichloromethane (anhydrous HPLC grade) was used as supporting electrolyte. For the measurements, silver reference electrode was calibrated against ferrocene/ferrocenium (Fc/Fc⁺) redox couple as an internal standard [20]. The theoretical calculations were carried out using the Gaussian 09 quantum chemical package [21]. Full geometry optimizations of the compounds in their electronic ground state were performed with DFT using the B3LYP functional consisting of Becke's three parameter hybrid exchange functional combined with the Lee-Yang-Parr correlation functional with the 6-31G (d, p) basis set in vacuum. The energies of the highest occupied (HOMO) and the lowest unoccupied (LUMO) molecular orbitals were obtained from single point calculations in the framework of DFT B3LYP/6-31G (d, p) method in vacuum. The ionization potentials of the solid samples of the compounds were estimated by the electron photoemission spectrometry in air [22,23]. The samples were fabricated by means of vacuum deposition of the materials at vacuum > 3×10⁻⁶ mbar onto fluorine doped tin oxide coated glass substrates. A deep-UV deuterium light source ASBN-D130-CM, a CM110 1/8m monochromator, a 6517B Keithley electrometer were included to the experimental setup which was similar to the previously described [24]. The charge-transporting properties of the compounds were investigated by the time of flight (TOF) and by charge extraction by linearly increasing voltage (Photo-CELIV) techniques [25,26]. The samples for TOF measurements were prepared depositing thick layers of materials by vacuum deposition on pre-patterned and pre-cleaned glass/indium tin oxide (ITO) substrates, using aluminium as top electrode. Similarly, the layers were deposited for the Photo-CELIV measurements. The TOF and Photo-CELIV experiments were performed as described earlier [27,28]. The TOF charge motilities were estimated using the formula $\mu = d^2/(V \times t_{tr})$, where *d* is the thickness of the layer, *V* is the applied voltage to a sample and *t_{tr}* is the transit time, which was taken from the photocurrent transients rebuilt in log-log scales. Photo-CELIV mobilities of the compounds were calculated

using the equation $\mu = 2d^2/3At_{\max}^2$; where d is the thickness of the film, $A = U(t)/t$ is the voltage rise rate, t_{\max} is the extraction time at the maxima of photocurrent transients [23]. PhOLEDs were fabricated depositing layer by layer at vacuum exceeding 3×10^{-6} mbar, utilizing vacuum equipment from Kurt J. Lesker in-built in an MB EcoVap4G glove box. PhOLEDs with the following architectures were fabricated: ITO/MoO₃ (3 nm)/*m*-MTDATA (50 nm)/95 wt% host (**3**, **5** or **6**):5 wt% Flrpic (15 nm)/TPBi (25 nm)/BCP (3 nm)/Ca (15 nm)/Al (120 nm) and ITO/MoO₃ (3 nm)/NPB(50 nm)/95 wt% host (**3**, **5** or **6**):5 wt% Flrpic (15 nm)/TPBi (25 nm)/Ca (15 nm)/Al (120 nm) (devices A (AI), B (BI) and C (CI) were based on hosts **3**, **5** and **6**, respectively). The ITO-coated glass substrates with a sheet resistance of 15 Ω /sq were patterned and then cleaned in acetone and isopropyl alcohol ultrasonic baths during ca. 10 min before deposition of the layers. The current density–voltage characteristics of the PhOLEDs were recorded by a Keithley source meter 2400 and the current density–luminance characteristics were recorded by a calibrated silicon photodiode with the 6517B Keithley electrometer. The photodiode was placed in front of PhOLEDs, assuming a Lambertian distribution of the electroluminescence (EL) of the devices. EL spectra were recorded by an Avantes AvaSpec-2048XL spectrometer while current, power, and external quantum efficiencies were calculated from the luminance, current density, and EL spectrum.

2.3. Synthesis

9-{4-[Bis(5-methoxy-1H-indol-3-yl)methyl]phenyl}-9H-carbazole (**2**). 5-Methoxyindole (**1**) (1.42 g, 9.6 mmol) and concentrated hydrochloric acid (2 ml) were slowly added to tetrahydrofuran (1.1 ml) and methanol (11 ml) solution of 4-(9H-carbazol-9-yl)benzaldehyde (**1**) (0.99 g, 3.6 mmol), and the mixture was stirred for 2 h at room temperature. The resulting solution was poured into water and filtered. The precipitate was dissolved in ethylacetate and washed with 10% NaOH

solution. The separated organic layer was dried over anhydrous Na_2SO_4 . The crude product was purified by crystallization from diethyl ether to afford the product as bright yellow crystals. Yield 1.52 g, 76%. ^1H NMR spectrum (300 MHz, DMSO, δ , ppm): 10.76 (s, 2H, NH), 8.23 (d, $J = 7.7$ Hz, 2H, Ar), 7.67 (d, $J = 8.3$ Hz, 4H), 7.53 (d, $J = 8.3$ Hz, 2H, Ar) 7.44-7.22 (m, 8H, Ar), 6.99 (d, $J = 2.3$ Hz, 2H, Ar), 6.86 (d, $J = 2.3$ Hz, 2H, Ar), 6.74 (dd, $J_1 = 8.3$ Hz $J_2 = 2.3$ Hz, 2H, Ar), 5.94 (s, 1H, CH), 3.64 (s, 6H, CH_3). ^{13}C NMR spectrum (75.4 MHz, DMSO, δ , ppm): 153.8, 140.7, 131.4, 130.1, 127.4, 126.6, 125.7, 124.4, 123.3, 120.2, 119.5, 118.7, 112.2, 111.6, 109.7, 101.9, 55.8, 40.1. IR (KBr, cm^{-1}): 3416 (NH); 3052 (C-H, Ar); 2993, 2936, 2829 (C-H); 1624, 1582 (C=C Ar); 1512, 1482 (C=C, Ar and C-H); 1452, 1439 (OCH_3); 1360, 1335, 1315 (C-N, Ar); 1211 (C-N); 797, 773, 751, 715, 625 (C-H Ar). MS (APCI⁺, 20 V), m/z : 549 ($[\text{M}+\text{H}]^+$). Anal. Calcd. for $\text{C}_{37}\text{H}_{29}\text{N}_3\text{O}_2$: C, 81.15; H, 5.34, N, 7.67; O, 5.84%; found C 81.22, H 5.33, N 7.62%.

9-{4-[Bis(1-ethyl-5-methoxy-1H-indol-3-yl)methyl]phenyl}-9H-carbazole (3). To a 250 ml three-necked flask containing compound **2** (0.3 g, 0.55 mmol) and tetra-*n*-butylammonium bromide (~0.1 g) in acetone (10 ml), 1-bromoethane (0.16 ml, 0.24 g, 2.2 mmol) and NaOH (0.21 g, 3.7 mmol) were added. The mixture was reflux for 3 h. Then the reaction mixture was poured into water, extracted with ethyl acetate (60 ml), washed with brine and deionized water, and dried over MgSO_4 . After filtration and evaporation of the solvent, the resulting white crystals were dissolved in hexane and purified by flash column chromatography using hexane/ethyl acetate (5:1, v/v) as an eluent. The product was obtained as white crystals. It was recrystallized from the eluent mixture of solvents. Yield 0.14 g (41%). ^1H NMR spectrum (300 MHz, CDCl_3 , δ , ppm): 8.14 (d, $J = 8.3$ Hz, 2H, Ar), 7.58 (d, $J = 8.3$ Hz, 2H, Ar), 7.48 (d, $J = 8.3$ Hz, 2H, Ar), 7.45-7.36 (m, 4H, Ar), 7.28-7.23 (m, 4H, Ar), 6.94-6.83 (m, 4H, Ar), 6.70 (s, 2H, Ar), 5.89 (s, 1H, CH), 4.09-4.02 (m, 4H, CH_2), 3.72 (s, 6H, OCH_3), 1.40 (t, $J = 7.2$ Hz, 6H, CH_3). ^{13}C NMR spectrum (75.4 MHz, CDCl_3 , δ , ppm): 153.5, 143.9, 135.4, 140.7, 131.8, 130.1, 127.9, 127.2, 126.7, 125.8, 123.3, 120.5, 119.7, 117.2, 111.8, 110.1, 109.7, 102.2, 55.9, 41.3, 40.1, 15.6. IR (KBr, cm^{-1}): 3046 (C-H, Ar); 2972, 2931,

2827 (C-H); 1619, 1575 (C=C Ar); 1512, 1487 (C=C, Ar and C-H); 1451, 1396 (OCH₃); 1351, 1335, 1314 (C-N, Ar); 1219 (C-N); 792, 750, 724, 711, 623 (C-H Ar). MS (APCI⁺, 20 V), m/z: 605 ([M+H]⁺). Anal. Calcd. for C₄₁H₃₇N₃O₂: C, 81.56; H, 6.18, N, 6.96; O, 5.30%; found C 81.51, H 6.24, N 7.03%.

9-{4-[Bis(2-phenyl-1*H*-indol-3-yl)methyl]phenyl}-9*H*-carbazole (**4**). The synthesis of compound **4** was carried out as described for compound **3** using 2-phenylindole (**II**) (0.74 g, 3.84 mmol), 4-(9*H*-carbazol-9-yl)benzaldehyde (0.42 g, 1.54 mmol). The crude product was purified by crystallization from acetone to afford the product as white crystals. Yield 1.81 g, 74%. ¹H NMR spectrum (300 MHz, DMSO, δ, ppm): 11.44 (s, 2H, NH), 8.24 (d, *J* = 7.7 Hz, 2H, Ar), 7.56-7.33 (m, 14H, Ar), 7.32-7.21 (m, 8H, Ar), 7.05 (dd, 4H, *J*₁ = 16.2 Hz, *J*₂ = 7.7 Hz, Ar), 6.78 (t, 2H, *J* = 7.7 Hz, Ar), 6.15 (s, 1H, CH). ¹³C NMR spectrum (75.4 MHz, DMSO, δ, ppm): 140.7, 136.8, 136.1, 135.0, 133.2, 130.9, 128.7, 127.8, 127.1, 126.7, 123.2, 121.6, 121.1, 120.3, 119.1, 114.3, 111.9, 110.0, 67.4, 25.5. IR (KBr, cm⁻¹): 3395 (NH); 3052 (C-H, Ar); 2975, 2869 (C-H); 1598, 1575 (C=C Ar); 1593, 1513, 1453 (C=C, Ar and C-H); 1364, 1355, 1313 (C-N, Ar); 1230 (C-N); 791, 743, 698, 626 (C-H Ar). MS (APCI⁺, 20 V), m/z: 640 ([M+H]⁺). Anal. Calcd. for C₄₇H₃₃N₃: C, 88.23; H, 5.20, N, 6.57%; found C 88.18, H 5.26, N 6.62%.

9-{4-[Bis(1-ethyl-2-phenyl-1*H*-indol-3-yl)methyl]phenyl}-9*H*-carbazole (**5**). The synthesis of compound **5** was carried out as described for compound **3** using compound **4** (0.72 g, 1.13 mmol), 1-bromoethane (0.67 ml, 0.98 g, 9 mmol) and tetra-*n*-butylammonium bromide (~0.2 g), KOH (0.21, g 3.7 mmol). The crude product was purified by crystallization from acetone to afford the product as white crystals. Yield 0.51 g, 65%. ¹H NMR spectrum (300 MHz, CDCl₃, δ, ppm): 8.12-8.05 (m, 2H, Ar), 7.54-7.38 (m, 7H, Ar), 7.34-7.32 (m, 4H, Ar), 7.30-7.24 (m, 4H, Ar), 7.18-7.12 (m, 7H, Ar), 6.92-6.88 (m, 6H, Ar), 5.72 (s, 1H, CH), 3.99-3.80 (m, 4H, CH₂), 1.15 (t, *J* = 7.1 Hz, 6H, CH₃). ¹³C NMR spectrum (75.4 MHz, CDCl₃, δ, ppm): 144.7, 141.1, 138.2, 135.8, 135.3, 132.3, 130.6, 127.7, 126.5, 125.8, 123.2, 121.1, 120.6, 120.3, 119.4, 119.2, 115.3, 109.9, 109.3,

40.2, 38.4, 15.4. IR (KBr, cm^{-1}): 3045 (C-H, Ar); 2970, 2929, 2870 (C-H); 1671, 1595 (C=C Ar); 1511, 1487 1451, (C=C, Ar and C-H); 1379, 1346, 1333, 1314 (C-N, Ar); 1233 (C-N); 742, 722, 701, 671, 620 (C-H Ar). MS (APCI⁺, 20 V), m/z : 697 ([M+H]⁺). Anal. Calcd. for C₅₁H₄₁N₃: C, 88.02; H, 5.94, N, 6.04%; found C 87.95, H 6.01, N 5.99%.

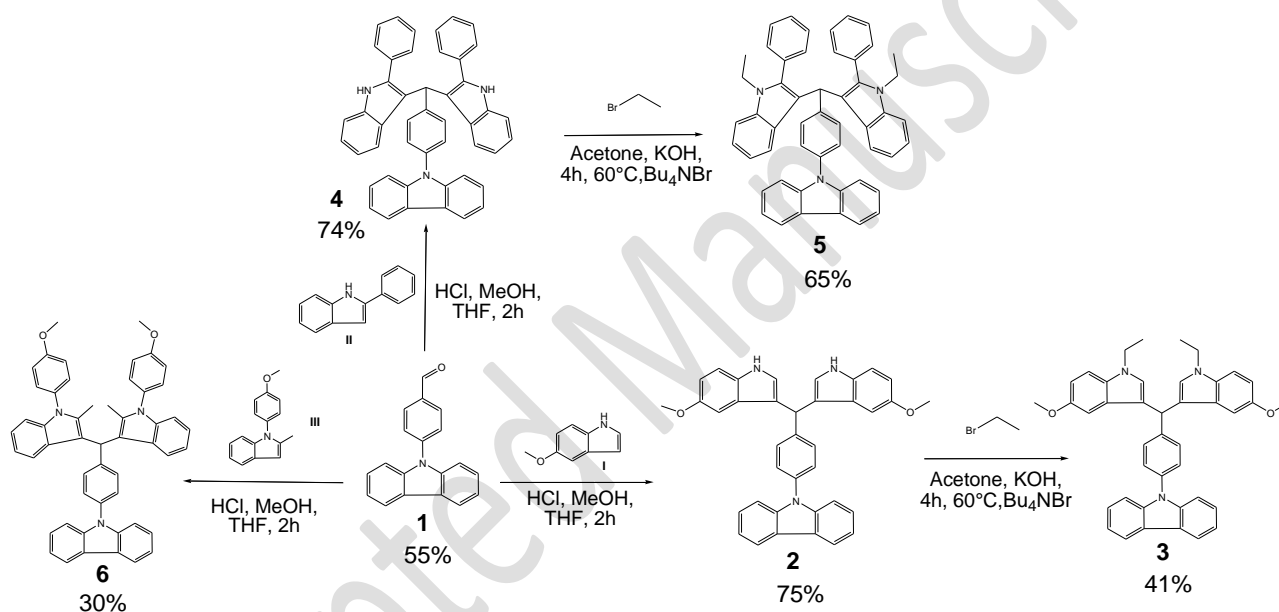
9-{4-[Bis(1-(4-methoxyphenyl)-2-methyl-1H-indol-3-yl)methyl]phenyl}-9H-carbazole (**6**). The synthesis of compound **6** was carried out as described for compound **3** using 4-(9H-carbazol-9-yl)benzaldehyde (**1**) (0.52 g, 1.88 mmol), 1-(4-methoxyphenyl)-2-methyl-1H-indole (**III**) (1.12 g, 4.7 mmol). The crude product was purified by crystallization from acetone to afford the product as white crystals. Yield 0.42 g, 30%. ¹H NMR spectrum (300 MHz, CDCl₃, δ , ppm): 8.14 (d, $J = 7.7$ Hz, 2H, Ar), 7.61 (d, $J = 8.3$ Hz, 2H, Ar), 7.51-7.37 (m, 6H, Ar), 7.25 (dd, $J_1 = 8.3$ Hz, $J_2 = 7.7$ Hz, 6H, Ar), 7.13-7.00 (m, 10H, Ar), 6.99-6.92 (m, 2H, Ar), 6.26 (s, 1H, CH), 3.88 (s, 6H, CH₃), 2.11 (s, 6H, CH₃). ¹³C NMR spectrum (75.4 MHz, CDCl₃, δ , ppm): 159.1, 143.5, 141.7, 138.6, 135.4, 134.4, 130.6, 129.5, 128.1, 126.9, 125.8, 123.3, 120.6, 120.3, 119.7, 119.4, 114.3, 113.4, 109.7, 55.5, 39.8. IR (KBr, cm^{-1}): 3044 (C-H, Ar); 2954, 2923, 2839 (C-H); 1606, 1595 (C=C Ar); 1513, 1478 (C=C, Ar and C-H); 1452, 1400 (OCH₃); 1346, 1334, 1317 (C-N, Ar); 1244 (C-N); 791, 750, 724, 669, 624 (C-H Ar). MS (APCI⁺, 20 V), m/z : 729 ([M+H]⁺). Anal. Calcd. for C₅₁H₄₁N₃O₂: C, 84.15; H, 5.68, N, 5.77; O, 4.40%; found C 84.11, H 5.73, N 5.75%.

3. Results and Discussion

3.1. Synthesis and thermal properties

Synthesis of compounds **3**, **5**, **6** containing electronically isolated indolyl moieties is outlined in Scheme 1. The starting compound 4-(9-carbazolyl)benzaldehyde (**1**) was prepared procedure well described in the literature [20]. The aldehyde **1** was then reacted with an excess of 5-methoxyindole

(**I**), 2-phenylindole (**II**) or 1-(4-methoxyphenyl)-2-methyl-1*H*-indole (**III**) to respectively produce compounds **2**, **4**, and **6**. Compounds **3** and **5** were synthesised by alkylation of **2** and **4** in the presence of potassium hydroxide. The target compounds were isolated after column chromatography and recrystallization as white crystalline solids. The chemical structures of the compounds were proved by NMR and IR and mass spectrometries and elemental analysis. The obtained compounds were found to be soluble in common organic solvents, such as tetrahydrofuran (THF), acetone and chloroform.



Scheme 1. Synthesis of compounds **3**, **5**, **6**.

The behavior under heating of compounds **3**, **5**, **6** was studied by TGA and DSC under the nitrogen atmosphere. The values of glass transition temperatures (T_g), melting points (T_m), and 5% weight loss temperatures ($T_{ID-5\%}$) are summarized in Table 1. All the compounds were obtained as crystalline materials as confirmed by DSC. They showed melting signals in the initial heating scans. The thermograms of derivative **5** are shown in Fig. 1a as an example. The crystalline sample of **5** showed endothermic melting signal at 169 °C on first heating and did not show any signal of crystallization upon cooling. When the amorphous sample was heated again, the glass transition

was observed at 108 °C and on further heating no peaks due to crystallization and melting appeared. The crystalline samples of derivatives **3** and **6** demonstrated analogous behavior during the DSC experiments. When the crystalline samples were heated during the DSC tests, endothermic peaks due to melting were observed at 115 and 167 °C. When the samples were cooled down and reheated, the glass-transitions were observed at 130 and 89 °C and, upon further heating no peaks due to crystallization and melting appeared. Our investigation confirmed that the crystalline derivatives **3**, **5**, **6** can be converted into an amorphous materials and used for the preparation of thin amorphous layers on substrates. The synthesized materials demonstrated high thermal stability as it was confirmed by TGA. The initial (5%) weight losses were recorded at 370 °C for **3**, at 405 °C for **5** and at 412 °C for **6** (Fig 1b). The values of $T_{ID-5\%}$ of **5** and **6** containing phenylindole moieties showed higher $T_{ID-5\%}$ compared to $T_{ID-5\%}$ of **3** containing indole moiety moiety. This observation indirectly shows that the thermal degradation of compound **3** started from the decomposition of indole moiety having ethyl and methoxy substituents.

Table 1. Temperatures of thermal transitions of compounds **3**, **5**, **6**.

Compound	T_g , [°C] (2 nd heating)	T_m , [°C]	$T_{ID-5\%}$, [°C]
3	89	115	370
5	108	169	405
6	130	167	412

Determined by DSC, scan rate 10 °C/min, N₂ atmosphere. T_m is melting point, T_g is glass transition temperature. $T_{ID-5\%}$ is 5% weight loss temperatures; scan rate 20 °C/min, N₂ atmosphere.

<Insert Fig.1>

3.2. Photophysical properties

Fig. 2a shows absorption spectra of the solutions of compounds **3**, **5**, **6** in THF (10^{-5} M) recorded at room temperature. The wavelengths of absorption maxima are summarized in Table 2. For the comparison, the UV-vis spectra of 9-phenylcarbazole and of the derivatives of indole (I-III) are given in Fig. 2a. Two absorption bands with the maxima at 293, 342 nm of compounds **3**, **5**, **6** can be attributed to π - π^* transition of 9-phenylcarbazole moieties. The energy band gaps were evaluated from the onsets of absorption spectra and were found to be even (3.53 eV) for all the compounds (**3**, **5**, **6**). Fig. 2b shows the normalized photoluminescence spectra of the dilute solutions of **3**, **5**, **6** in THF (10^{-5} M) recorded under excitation wavelength of 350 nm. The compounds showed short and identical Stokes shifts of 24 nm. The photoluminescence spectra were also recorded at the temperature of liquid nitrogen (without gate delays). The wavelengths of fluorescence peaks of the solutions of **3**, **5**, and **6** were identical both at 77 K and at room temperatures indicating the absence of the charge transfer (Fig. 2b). The absolute fluorescence quantum yields of the solutions of **3**, **5**, **6** in THF ranged from 22.9 to 44.2%. To separate phosphorescence spectra from fluorescence of compounds **3**, **5**, **6**, emission spectra were also measured with gate delays (> 50 ms). The phosphorescence spectra of compounds **3** and **6** exhibited similar peak positions corresponding the first triplet energy level (E_T) of 3.06 eV. The shapes of phosphorescence spectra for all the compounds were similar; however, the phosphorescence maximum of compound **5** was shifted to the longer wavelengths comparing to phosphorescence maxima of derivatives **3** and **6**. This observation can apparently be explained by the intramolecular interaction in **5**. The calculated values of E_T were found to be 3.03 eV for **3**, 2.65 eV for **5** and 3.02 eV for **6**, which match well with the experimental values (Table 2).

Table 2. Photophysical properties of compounds **3**, **5**, **6**.

Compound	λ_{abs} , [nm] ^a	λ_{PI} , [nm] ^c	Stokes shift, [nm] ^d	Φ_{F} , [%] ^e	E_{T} , [eV] ^f	E_{T} , [eV] ^g	E_{g} , [eV] ^h
3	261, 287 ^b , 293, 342	350, 366	24	39.8	3.06	3.03	3.53
5	261, 287 ^b , 293, 342	350, 366	24	44.2	2.70	2.65	3.53
6	261, 287 ^b , 293, 342	350, 366	24	22.9	3.06	3.02	3.53

^a λ_{abs} are the wavelength of absorption maxima of the solutions in THF. ^b Shoulder peak. ^c λ_{PI} are the wavelengths of emission maxima of the solutions in THF. ^d $\lambda_{\text{PI}} - \lambda_{\text{abs}}$. ^e Absolute quantum yield of THF solution. ^f Estimated from set-on of phosphorescence spectra (calculated from $1240/\lambda_{\text{PI}}$). ^g Theoretically calculated triplet energy level. ^h Optical band gap calculated from $1240/\lambda_{\text{abs}}^{\text{onset}}$ (onset absorption).

<Insert Fig.2>

3.3. Electrochemical and electron photoemission properties

The electrochemical properties of the derivatives **3**, **5**, **6** were studied by cyclic voltammetry (CV). The oxidation potential, ionization potential (IP_{CV}) and electron affinity (EA_{CV}) values of compounds **3**, **5**, **6** are compiled in Table 3. Cyclic voltammograms of **3** are shown in Fig. 3a. Compounds **3**, **5**, **6** were found to be electrochemically stable. They exhibited two irreversible oxidation peaks with the onsets at 0.95 V and 1.35 V in the repeated cycles of redox processes up to 1.5 V which can be attributed to the formation of radical cations. During the multiple scans of compound **3** its CV curve retained its shape. The similar CV curves were observed for compounds **5** and **6** (Fig. S1). The IP_{CV} values of compounds **3**, **5**, **6** were found to be comparable (5.61, 5.74, and 5.72 eV, respectively). The EA_{CV} values of the compounds were found to be -2.08, -2.21, -2.19 eV, correspondingly.

Table 3. Oxidation potential, IP_{EP} , IP_{CV} , IP_{vert} , E_{ACV} , HOMO and LUMO energy values of **3**, **5**, **6**.

Compound	E_{onset}^{ox} vs Fc, [V]	IP_{CV} , [eV] ^a	E_{ACV} , [eV] ^a	IP_{EP} , [eV] ^b	IP_{vert} , [eV] ^c	HOMO, [eV] ^d	LUMO, [eV] ^e
3	0.51	5.61	-2.08	5.72	5.99	-4.93	-0.56
5	0.64	5.74	-2.21	5.68	5.89	-5.08	-0.60
6	0.62	5.72	-2.19	5.70	5.96	-4.98	-0.49

^a $IP_{CV} = -(E_{onset}^{ox} + 5.1)$ [29]; $E_{ACV} = E_g - IP_{CV}$ (where, E_{onset}^{ox} are onset reduction and oxidation potentials versus the Fc^+/Fc). ^b Estimated from electron photoemission spectra. ^c Theoretically calculated by the DFT B3LYP/6-31G (d, p) approach in vacuum. ^d Theoretically calculated HOMO energy. ^e Theoretically calculated LUMO energy.

<Insert Fig.3>

In addition, we estimated the solid-state ionization potentials (IP_{EP}) by electron photoemission (EP) method in air (Fig. 3b, Table 3). Ionization potentials of compounds **3**, **5**, and **6** were found to be comparable (*ca.* 5.7 eV). These IP_{EP} values are close to the HOMO of blue phosphorescent emitter FIrpic. The values of ionization potentials established by the two methods practically coincided. The differences did not exceed 0.11 eV.

3.4. Theoretical calculations

Molecular simulations were carried out to better understand the electron distributions and energy levels of the three host materials. Quantum chemical calculations for compounds **3**, **5**, and **6** were performed using 6-31G (d, p) basis set as a starting point. Our calculations show that the

optimal neutral electronic ground state geometries are not planar for the molecules of **3**, **5**, and **6**. It was found, that the value of dihedral angles are 43.89, 43.98 and 44.16° for **3**, **5**, and **6**, respectively. The geometry optimizations for the molecules of **3**, **5**, and **6** can be found in Fig. S2. The electron densities of the first and second highest occupied molecular orbitals (HOMO, HOMO-1) and the first, second lowest unoccupied molecular orbitals (LUMO, LUMO+1) in vacuum state are depicted in Fig. 4, Fig. S2. π -Electrons in the HOMO orbital of the derivative **5** are delocalized over all carbazole-indole backbone, whereas the HOMO orbital of the derivatives **3** and **6** are delocalized over one and two indolyl moieties, respectively with very close energy levels. While the HOMO-1 orbitals of the **3** and **5** are delocalized over one and two indolyl moieties, respectively, HOMO-1 orbital of **6** is delocalized on carbazolyl and phenyl moieties. The LUMO orbitals of **3**, **5**, and **6** are only delocalized on carbazolyl moieties. The LUMO+1 of **6** is delocalized on 4-methoxyphenyl moiety, while those of **3** and **5** are delocalized over indolyl and the linking phenyl moieties. At the Hartree-Fock level, Koopmans theorem suggests that the energy of the HOMO is a good approximation to the negative experimental ionization potential (-IP) [30]. As it can be seen from the data of Table 3, the absolute values of experimentally and theoretically estimated IP and HOMO energy are comparable. The values of HOMO energy increases in the range of $\mathbf{5} < \mathbf{6} < \mathbf{3}$.

<Insert Fig.4>

The theoretical UV-vis spectra for compounds **3**, **5**, **6** (Fig. S3), simulated from the oscillator strengths of singlet transitions calculated by the time-dependent version of DFT method (TD-DFT) B3LYP/6-31G (d, p) method in vacuum, indicate that the absorption maxima at 295, 327 and 315 nm, respectively are dominated by $S_0 \rightarrow S_1$ electronic transitions, with the oscillator strengths of 0.192 for **3**, of 0.036 for **5** and of 0.045 for **6**.

The ionization potentials of the solid layers of the synthesized compounds estimated by electron photoemission method (IP_{EP}) were compared with vertical ionization potentials, © 2018. This manuscript version is made available under the CC-BY-NC-ND 4.0 license <http://creativecommons.org/licenses/by-nc-nd/4.0/>

theoretically calculated in the framework of the DFT B3LYP/6-311G (d, p) approach which are given in Table 3. As it can be seen from Table 3, The trends of the theoretical vertical ionization potentials of **3**, **5**, **6** (5.99, 5.89 and 5.96 eV, respectively) were found to be the same as for IP experimentally estimated by electron photoemission spectrometry.

3.5. Charge-transporting properties

Charge-transporting properties of the vacuum-deposited layers of compounds **3**, **5**, and **6** were investigated by TOF and by Photo-CELIV methods. The dependencies of the hole and electron drift mobilities on the square root of electric field for the layer of **5** are shown in Fig. 5A. The dependencies shows linear character with the good agreement to the Poole-Frenkel relationship $\mu = \mu_0 \times \exp(\alpha \times E^{1/2})$ [31]. The recorded hole and electron mobility values for the layer of compound **5** exceeded $1.3 \times 10^{-3} \text{ cm}^2/\text{Vs}$ at electric field higher than $8.1 \times 10^5 \text{ V/cm}$. The TOF and CELIV mobilities obtained for **5** were found to be in good agreement. The hole and electron TOF transients for the layer of compound **5** illustrating of dispersive hole and electron transport are shown in Fig. 5B,C. The transit times were not observed in the linear plots, however, they were found on log-log plots. The characteristic extraction time t_{max} , which is required for calculating Photo-CELIV mobility, was well seen in the hole and electron Photo-CELIV current transients as maximum at different voltage rise rates A , where $A = U(t)/t$, U is applied linearly increasing positive voltage of the pulse duration t (Fig. S4D,E). Using TOF and Photo-CELIV methods, transit times and the characteristic extraction time t_{max} for holes and electrons of the layers of compounds **3** and **6** were not found apparently due to the strong dispersity. Comparing chemical structures of the compound **5** with compounds **3** and **6**, the main difference for them is in methoxy substituents (Scheme 1). Methoxy groups can induce C–H \cdots π , O, N hydrogen bonds which can lead to the changes in intermolecular interaction energies [23].

<Insert Fig.5>

3.6. Performance in blue PhOLEDs

For the investigation of the performance of **3**, **5** and **6** as hosts, the simple PhOLEDs (devices A, B and C) were fabricated in the structures of which MoO₃ and *m*-MTDATA were used as the hole- injecting and transporting materials, TPBi and BCP were utilized as the electron transporting and injecting materials, respectively. To deposit the emitting layers **3**:FIrpic, **5**:FIrpic and **6**:FIrpic for the devices A, B and C, hosts **3**, **5** and **6** were doped with FIrpic as the blue phosphorescent emitter. Good charge balance in devices A, B and C was expected due to the well balanced hole and electron mobilities of **5** as well as due to the multilayer structures of PhOLEDs in which the additional and emitting layers with appropriate HOMO and LUMO levels were selected (Fig. 6 a). In addition, because of the relatively high triplet levels of **3**, **5** and **6** (Table 2), efficient exciton confinement on the dopant FIrpic was expected [32].

<Insert Fig.6>

<Insert Fig.7>

The brightness and efficiency characteristics of the devices A, B and C are plotted in Fig. 7. Confirming efficient injection from the electrodes and transport of holes and electrons to the emitting-layer, relatively low values of the turn-on voltages of 3.5, 3.7 and 3.0 V (at 1 cd/m²) were observed for the devices A, B and C, respectively. Much lower maximum brightness of *ca.* 2600 cd/m² was observed for device A than for devices B (8300 cd/m²) and C (4500 cd/m²) (Fig. 7a) indicating worse performance of host **3** relative to hosts **5** and **6**. The lower value of maximum external quantum efficiency (EQE) of 1.1% was observed for device A relative to devices B (EQE = 7.5%) and C (EQE = 5.8%) (Fig. 7 d). This observation shows more effective exciton

© 2018. This manuscript version is made available under the CC-BY-NC-ND 4.0 license
<http://creativecommons.org/licenses/by-nc-nd/4.0/>

recombination as well as radiative transition in the emitting layers with the hosts **5** and **6** compared to the emitting layer with the host **3** [33]. The lower output parameters of device A could be mostly due to the less efficient energy transfer from host **3** to FIrpic comparing to that from hosts **5** and **6** to FIrpic. In contrast to devices B and C, the emission in high-energy blue region, which was not related to that of FIrpic, was observed in the EL spectrum of devices A (Fig. 8) showing inefficient energy transfer from **3** to FIrpic. This is apparently the main reason of low EQE of the device A. Another reason could be the considerable charge transport dispersity, which was observed by TOF measurement, for **3**, resulting in disbalance of charges in the emitting layer. The maximum EQE of device B and C is comparable to those of the reported PhOLEDs with the similar structure [8,9,34,35,36]. The better performance of the blue PhOLEDs using compounds **5** and **6** as the host can apparently be reached after the optimization of the concentration of FIrpic in emitting layer, optimization of the thicknesses of the layers of the device or after introduction of the additional layers. It also would be of interest to modify compounds **5** and **6** by the attachment of accepting high-triplet-energy unit which could improve the charge balance.

The PhOLED structures were additionally optimized. We additionally fabricated PhOLEDs (devices AI, BI and CI) in which *m*-MTDATA was replaced by NPB and the layer of BCP was skipped compared to the structures of devices A, B and C. The optimization allowed to decrease the energy barriers for holes and electrons in devices A, B and C (Fig. 6 b). The electroluminescence (EL) spectra of devices AI, BI and CI were very similar to those of devices A, B and C due to the same FIrpic emitter used. The brightness and efficiency characteristics of devices AI, BI and CI are plotted in Fig. 7. The improved turn-on voltages of 2.4 and 2.7 V (at 1 cd/m²) were observed for devices BI and CI, respectively. The values of maximum external quantum efficiency of 18 and 14.8%, which are comparable to those published before [32], were obtained for devices BI and CI showing that optimization was very effective. Practically, no improvement of maximum EQE was observed for the optimized device AI (Fig. 7d). The results of characterization of devices A, B and

C also show that compounds **5** and **6** are more efficient hosts for the structured blue PhOLEDs than compound **3**.

The EL spectra of the devices A, B and C recorded at the different applied voltages are shown in Fig. 8a-c. Since Flrpic was used as the phosphorescent emitter in all devices, the similar shapes of EL spectra were observed for the PhOLEDs exhibiting intensity peaks at *ca.* 473 and 495 nm which can be apparently attributed to the monomer emission peaks of Flrpic (Fig. 8 a-c). As it was mentioned above, low intensity high-energy blue emission with the intensity maximum at *ca.* 425 nm was observed in EL spectra of device A. The wavelength of this emission band was close to that of photoluminescence of *m*-MTDATA showing that the recombination of excitons occurred not only in the emitting layer but also in the hole-transporting layer of device A. The additional electron-blocking layer and exciton-blocking layer are required for avoiding the recombination of excitons in the hole-transporting layer [37]. The shapes of EL spectra for all devices was very stable at different applied voltages showing absence of exciplex, electromer or electroplex emission [38] which would decrease the efficiency and color-purity of one color PhOLEDs.

<Insert Fig.8>

Conclusions

A series of derivatives containing carbazolyl and indolyl moieties were synthesized and their thermal, optical, photophysical, electrochemical, photoelectrical and electroluminescent properties were studied. The synthesized compounds were found to be thermally stable with 5 % weight loss temperatures of 370-412 °C. The formed molecular glasses with the glass transition temperatures ranging from 89 to 130 °C. The analysis of UV-vis spectra and oscillation strengths proved that the absorption bands of the compounds with the maxima at 295, 327 and 315 nm are dominated by

$S_0 \rightarrow S_1$ electronic transitions. The phosphorescence spectra of the dilute solutions of the compounds © 2018. This manuscript version is made available under the CC-BY-NC-ND 4.0 license <http://creativecommons.org/licenses/by-nc-nd/4.0/>

revealed high values of the first triplet energy level (up to 3.06 eV). The ionization potential and electron affinity values of the compounds established ranged from 5.61 to 5.74 eV, and from -2.09 to -2.08 eV, respectively. One compound exhibited well balanced hole and electron transport with charge mobilities reaching $1.3 \times 10^{-3} \text{ cm}^2/\text{V}\times\text{s}$ at electric fields higher than $8.1 \times 10^5 \text{ V/cm}$. Two compounds were tested as hosts in electrophosphorescent devices utilizing bis(4',6'-difluorophenylpyridinato)-iridium(III) picolinate as the emitting dopant. The best fabricated device showed turn-on voltage of 2.4 V (at 1 cd/m^2); maximum current efficiency of 44.7 cd/A, maximum brightness of 4500 cd/m^2 (at 7 V), maximum current efficiency of 38.6 lm/W, and external quantum efficiency of *ca.* 18 %.

Acknowledgments

This work was supported by the Horizon 2020 ICT29-2014 project PHEBE (grant No 641725).

Appendix A. Supplementary data

Supplementary data associated with this article can be found, in the online version, at <http://dx.doi.org/>

References

[1] (a) Fyfe D. LED technology, organic displays come of age. *Nat Photon* 2009;3:453-5; (b) Sanyin Q, Tian H. Diketopyrrolopyrrole (DPP)-based materials for organic photovoltaics. *Chem Commun* 2012;48:3039-51.

[2] Adachi C, Baldo MA, Thompson ME, Forrest SR. Nearly 100% internal phosphorescence efficiency in an organic light-emitting device. *J Appl Phys* 90 (2001) 5048-51.

© 2018. This manuscript version is made available under the CC-BY-NC-ND 4.0 license <http://creativecommons.org/licenses/by-nc-nd/4.0/>

- [3] Uoyama H, Goushi K, Shizu K, Nomura H, Adachi C. Highly efficient organic light-emitting diodes from delayed fluorescence. *Nature* 2012;492:23438.
- [4] Sato K, Shizu K, Yoshimura K, Kawada A, Miyazaki H, Adachi C. Organic luminescent molecule with energetically equivalent singlet and triplet excited states for organic light-emitting diodes. *Phys Rev Lett* 2013;110:247401-5.
- [5] Baldo M, O'Brien ADF, You Y, Shoustikov A, Sibley S, Thompson ME, et al. Highly efficient phosphorescent emission from organic electroluminescent devices. *Nature* 1998;395:151-4.
- [6] (a) Yook KS, Lee JY. Organic materials for deep blue phosphorescent organic light-emitting diodes. *Adv Mater* 2012;24:3169-90; (b) Ho CL, Chi LC, Hung WY, Chen WJ, Lin YC, Wu H. Carbazole-based coplanar molecule (CmInF) as a universal host for multi-color electrophosphorescent devices. *J Mater Chem* 2012;22:215-24; (c) Xu Huixia, Sun Peng, Wang Kexiang, Miao Yanqin, Yang Tingting, Wang Hua. 1,2,4-Triazole derivatives as host materials for blue and green phosphorescent organic light-emitting devices. *Tetrahedron* 2016;72:4408–13.
- [7] Wagner D, Hoffmann ST, Heinemeyer U, Munster I, Kohler A, Strohriegel P. Triazine based bipolar host materials for blue phosphorescent OLEDs. *Chem Mater* 2013;25:3758-65.
- [8] Dumur F, Beouch L, Peralta S, Wantz G, Goubard F, Gigmes D. Solution-processed blue phosphorescent OLEDs with carbazole-based polymeric host materials. *Org Electron* 2015;25:21-30.
- [9] Zhang Y, Lee J, Forrest SR. Tenfold increase in the lifetime of blue phosphorescent organic light-emitting diodes. *Nature Commun* 2014;5:1-7.

[10] (a) Dalal SS, Walters DM, Lyubimov I, de Pablo JJ, Ediger MD. Tunable molecular orientation and elevated thermal stability of vapor-deposited organic semiconductors. *PNAS* 2015;112:4227-32; (b) Xiang N, Gao Z, Tian G, Chen Y, Liang W, Huang J, et al. Novel fluorene/indole-based hole transport materials with high thermal stability for efficient OLEDs. *Dyes Pigm* 2017;137:36-42.

[11] Jou JH, Kumar S, Agrawal A, Li TH, Sahoo S. Approaches for fabricating high efficiency organic light emitting diodes. *J Mater Chem C* 2015;3:2974-3002.

[12] (a) Zhang L, Zhang YX, Hu Y, Shi XB, Jiang ZQ, Wang ZK, et al. Highly efficient blue phosphorescent organic light-emitting diodes employing a host material with small bandgap. *ACS Appl Mater Interfaces* 2016;8:16186-91; (b) Ho CL, Wong WY. Small-molecular blue phosphorescent dyes for organic light-emitting devices. *New J Chem* 2013;37:1665-83; (c) Dong Q, Lian H, Gao Z, Guo Z, Xiang N, Zhong Z. Novel spirofluorene/indole/carbazole-based hole transport materials with high triplet energy for efficient green phosphorescent organic light-emitting diodes *Dyes Pigm* 2017;137:84-90.

[13] Xiao L, Chen Z, Qu B, Luo J, Kong S, Gong Q, et al. Recent progresses on materials for electrophosphorescent organic light-emitting devices. *Adv Mater* 2011;23:926-52.

[14] (a) Cheng SH, Hung WY, Cheng MH, Chen HF, Lee GH, Chung CL, et al. Highly twisted carbazole-oxadiazole hybrids as universal bipolar hosts for high efficiency PhOLEDs. *Adv Electron Mater* 2016;2:500241; (b) Wong WY. Metallated molecular materials of fluorene derivatives and their analogues. *Coord Chem Rev* 2005;249:971-97.

[15] Kautny P, Wu Z, Eichelster J, Horkel E, Stoger B, Chen J, et al. Indolo[3,2,1-jk]carbazole based planarized CBP derivatives as host materials for PhOLEDs with low efficiency roll-off. *Org Electron* 2016;34:237-45.

[16] Huang JJ, Hung YH, Ting PL, Tsai YN, Gao HJ, Chiu TL, et al. Orthogonally substituted benzimidazole-carbazole benzene as universal hosts for phosphorescent organic light-emitting diodes. *Org Lett* 2016;18:672-5.

- [17] Zhang Z, Xie J, Wang Z, Shen B, Wang H, Li M, et al. Manipulation of electron deficiency of δ -carboline derivatives as bipolar hosts for blue phosphorescent organic light-emitting diodes with high efficiency at 1000 cd m⁻². *J Mater Chem C* 2016;4:4226-35.
- [18] Yang X, Lu R, Gai F, Xue P, Zhan Y. Rigid dendritic gelators based on oligocarbazoles. *Chem Commun* 2010;46:1088-90.
- [19] Verma AK, Singh J, Larock RC. Benzotriazole: an efficient ligand for the copper-catalyzed N-arylation of indoles. *Tetrahedron* 2009;65:8434-9.
- [20] Gagne RR, Koval CA, Lisensky GC. Ferrocene as an internal standard for electrochemical measurements. *Inorg Chem* 1980;19:2854-5.
- [21] Frisch MJ, Trucks GW, Schlegel HB, Scuseria GE, Robb MA, Cheeseman JR. et al. Gaussian 09, Revision A.02, Gaussian, Inc., Wallingford CT, 2009.
- [22] Miyamoto E, Yamaguchi Y, Yokoyama M. Ionization potential of organic pigment film by atmospheric photoelectron emission analysis, *Denshishashin Gakkai-shi (Electrophotography)* 1989;28:364-70.
- [23] (a) Gudeika D, Grazulevicius JV, Volyniuk D, Butkute R, Juska G, MiasojedovasA, et al. Structure-properties relationship of the derivatives of carbazole and 1,8-naphthalimide: effects of the substitution and the linking topology. *Dyes Pigm* 2015;114:239-52; (b) Lukstaite J, Gudeika D, Grazulevicius JV, Grigalevicius S, Zhang B, Xie Z. Copolymers containing electronically isolated indolyl fragments as materials for optoelectronics. *React Funct Polym* 2010;70:572-7.

- [24] Gudeika D, Grazulevicius JV, Volyniuk D, Juska G, Jankauskas V, Sini G. Effect of ethynyl linkages on the properties of the derivatives of triphenylamine and 1,8-naphthalimide. *J Phys Chem C* 2015;119:28335-46.
- [25] Juska G, Nekrasas N, Valentinavicius V, Meredith P, Pivrikas A. Extraction of photogenerated charge carriers by linearly increasing voltage in the case of Langevin recombination. *Phys Rev B* 2011;84:155202-206.
- [26] Juška G, Arlauskas K, Viliūnas M, Kočka J. Extraction current transients: new method of study of charge transport in microcrystalline silicon. *Phys Rev Lett* 2000;84:4946-9.
- [27] Zilinskaite V, Gudeika D, Grazulevicius JV, Volyniuk D, Buika G, Jankauskas V, et al. Derivatives of indandione and differently substituted triphenylamine with charge-transporting and NLO properties. *Dyes Pigm* 2015;113:38-46.
- [28] Gudeika D, Sini G, Jankauskas V, Sych G, Grazulevicius JV. Synthesis and properties of the derivatives of triphenylamine and 1,8-naphthalimide with the olefinic linkages between chromophores. *RSC Advances* 2016;6:2191-201.
- [29] Cardona CM, Li W, Kaifer AE, Stockdale D, Bazan GC. Electrochemical considerations for determining absolute frontier orbital energy levels of conjugated polymers for solar cell applications. *Adv Mater* 2011;23:2367-71.
- [30] Cramer CJ, editor. *Essentials of computational chemistry: theories and models*. 2nd ed. Hoboken, NJ: Wiley; 2004, ISBN 978-0-470-09182-1 [Chapter 5].
- [31] Borsenberger PM, Shi J. Hole transport in a vapor deposited phenylenediamine molecular glass. *Phys Status Solidi B* 1995;191:461-9.
- [32] Gudeika D, Volyniuk D, Grazulevicius JV, Skuodis E, Yu SY, Liou WT, et al. Derivative of oxyfluorene and di-tert-butyl carbazole as the host with very high hole mobility for high-efficiency blue phosphorescent organic light-emitting diodes. *Dyes Pigm* 2016;130:298-305.

- [33] Zhang Z, Zhang Z, Ding D, Wei Y, Xu H, Jia J, et al. Selectively investigating molecular configuration effect on blue electrophosphorescent host performance through a series of hydrocarbon oligomers. *J Phys Chem C* 2014;118:20559-70.
- [34] Adachi C, Kwong RC, Djurovich P, Adamovich V, Baldo MA, Thompson ME, et al. Endothermic energy transfer: a mechanism for generating very efficient high-energy phosphorescent emission in organic materials. *Appl Phys Lett* 2001;79:2082-4.
- [35] Whang DR, You Y, Kim SH, Jeong WI, Park YS, Kim JJ, et al. A highly efficient wide-band-gap host material for blue electrophosphorescent light emitting devices. *Appl Phys Lett* 2007;91:233501-503.
- [36] Gong SL, He X, Chen YH, Jiang ZQ, Zhong C, Ma DG, et al. Simple CBP isomers with high triplet energies for highly efficient blue electrophosphorescence. *J Mater Chem* 2012;22:2894-9.
- [37] He G, Pfeiffer M, Leo K, Hofmann M, Birnstock J, Pudzich R, et al. High-efficiency and low-voltage p-i-n electrophosphorescent organic light-emitting diodes with double-emission layers. *Appl Phys Lett* 2004;85:3911-3.
- [38] Ban X, Sun K, Sun Y, Huang B, Ye S, Yang M, et al. High power efficiency solution-processed blue phosphorescent organic light-emitting diodes using exciplex-type host with a turn-on voltage approaching the theoretical limit. *ACS Appl Mater Interfaces* 2015;7:25129-38.

List

Scheme 1. Synthesis of compounds **3**, **5**, **6**.

Table 1. Temperatures of thermal transitions of compounds **3**, **5**, **6**.

Table 2. Photophysical properties of compounds **3**, **5**, **6**.

Table 3. Oxidation potential, IP_{EP} , IP_{CV} , IP_{vert} , E_{ACV} , HOMO and LUMO energy values of **3**, **5**, **6**.

Fig. 1. (a) DSC curves of compound **5**. (b) TGA curves of compounds **3**, **5**, **6**.

Fig. 2. (a) Absorption spectra of the dilute solutions of 9-phenylcarbazole, **I-III**, **3**, **5**, **6** in THF. (b) Photoluminescence (Pl) and phosphorescence (Ph) ($\lambda_{ex} = 350$ nm) spectra of the solutions of **3**, **5**, **6** in THF.

Fig. 3. Cyclic voltammograms of compound **3** (a) and electron photoemission spectra of the thin films of compounds **3**, **5**, **6** (b).

Fig. 4. Electron density distributions and the energy levels of compounds **3**, **5**, and **6** obtained by DFT calculation (B3LYP/6-31G (d, p)).

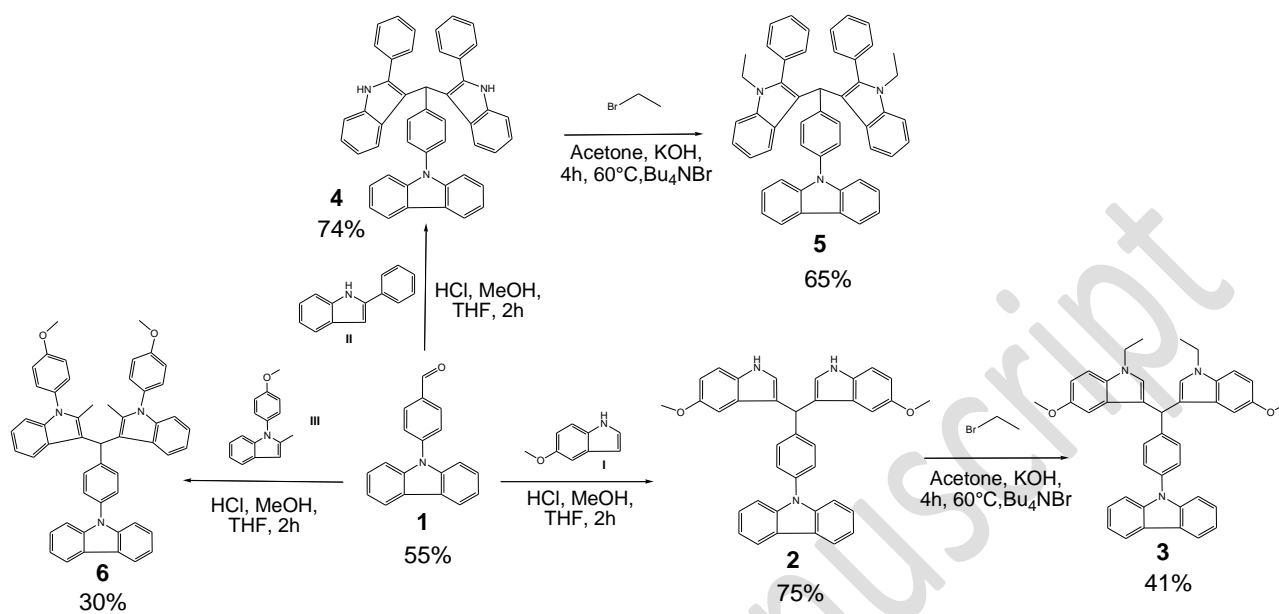
Fig. 5. Hole and electron drift mobility as a function of $E^{1/2}$ for the layer of **5** (A). TOF transient curves in the log-log scales (B, C).

Fig. 6. Energy level diagrams for the devices A, B, C (a) and AI, BI, CI (b).

Fig. 7. Current density and brightness versus voltage (a), current (d), power (c), and external quantum (d) efficiencies versus current density for studied devices.

Fig. 8. Electroluminescence spectra of the devices A (a), B (b) and C (c) recorded at the different applied voltages.

Scheme



Scheme 1. Synthesis of compounds **3**, **5**, **6**.

Tables

Table 1. Temperatures of thermal transitions of compounds **3**, **5**, **6**.

Compound	T _g , [°C] (2 nd heating)	T _m , [°C]	T _{ID-5%} , [°C]
3	89	115	370
5	108	169	405
6	130	167	412

Determined by DSC, scan rate 10 °C/min, N₂ atmosphere. T_m is melting point, T_g is glass transition temperature. T_{ID-5%} is 5% weight loss temperatures; scan rate 20 °C/min, N₂ atmosphere.

Table 2. Photophysical properties of compounds **3**, **5**, **6**.

Compound	λ _{abs} , [nm] ^a	λ _{PI} , [nm] ^c	Stokes shift, [nm] ^d	Φ _F , [%] ^e	E _T , [eV] ^f	E _T , [eV] ^g	E _g , [eV] ^h
3	261, 287 ^b , 293, 342	350, 366	24	39.8	3.06	3.03	3.53
5	261, 287 ^b , 293, 342	350, 366	24	44.2	2.70	2.65	3.53
6	261, 287 ^b , 293, 342	350, 366	24	22.9	3.06	3.02	3.53

^a λ_{abs} are the wavelength of absorption maxima of the solutions in THF. ^b Shoulder peak. ^c λ_{PI} are the wavelengths of emission maxima of the solutions in THF. ^d λ_{PI}-λ_{abs}. ^e Absolute quantum yield of THF solution. ^f Estimated from set-on of phosphorescence spectra (calculated from 1240/λ_{PI}). ^g Theoretically calculated triplet energy level. ^h Optical band gap calculated from 1240/λ_{abs}^{onset} (onset absorption).

Table 3. Oxidation potential, IP_{EP}, IP_{CV}, IP_{vert}, EA_{CV}, HOMO and LUMO energy values of **3**, **5**, **6**.

Compound	E _{onset} ^{ox} vs Fc, [V]	IP _{CV} , [eV] ^a	EA _{CV} , [eV] ^a	IP _{EP} , [eV] ^b	IP _{vert} , [eV] ^c	HOMO, [eV] ^d	LUMO, [eV] ^e
3	0.51	5.61	-2.08	5.72	5.99	-4.93	-0.56
5	0.64	5.74	-2.21	5.68	5.89	-5.08	-0.60
6	0.62	5.72	-2.19	5.70	5.96	-4.98	-0.49

^a IP_{CV} = -(E_{onset}^{ox} + 5.1) [30]; EA_{CV} = E_g - IP_{CV} (where, E_{onset}^{ox} are onset reduction and oxidation potentials versus the Fc⁺/Fc). ^b Estimated from electron photoemission spectra. ^c Theoretically calculated by the DFT B3LYP/6-31G (d, p) approach in vacuum. ^d Theoretically calculated HOMO energy. ^e Theoretically calculated LUMO energy.

Figures

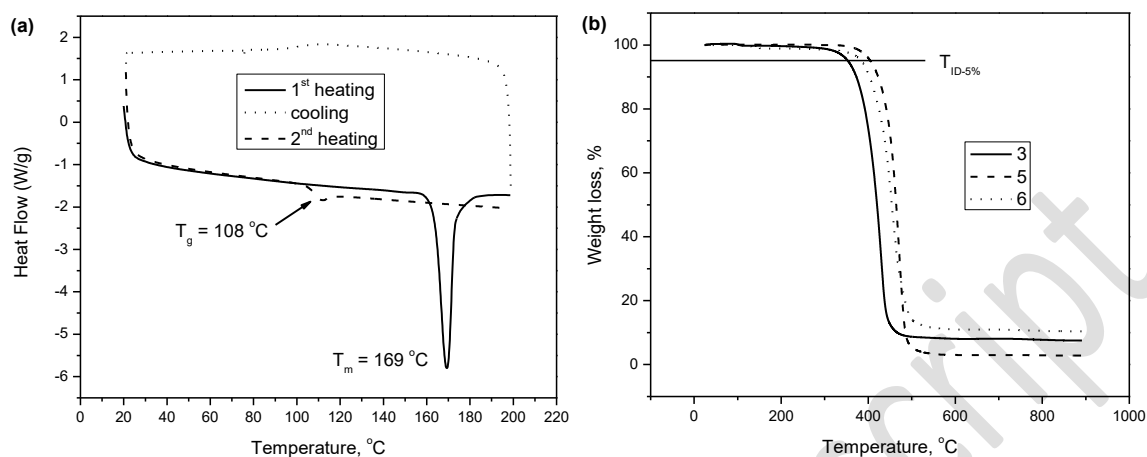


Fig. 1. (a) DSC curves of compound **5**. (b) TGA curves of compounds **3**, **5**, **6**.

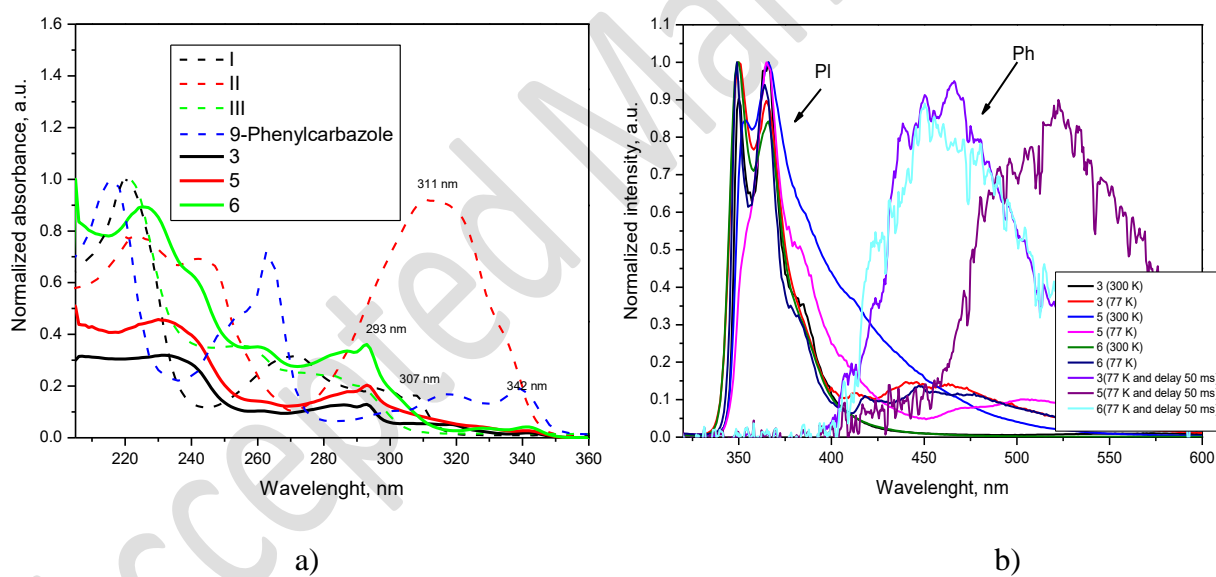


Fig. 2. (a) Absorption spectra of the dilute solutions of 9-phenylcarbazole, **I-III**, **3**, **5**, **6** in THF. (b) Photoluminescence (PI) and phosphorescence (Ph) ($\lambda_{\text{ex}} = 350$ nm) spectra of the solutions of **3**, **5**, **6** in THF.

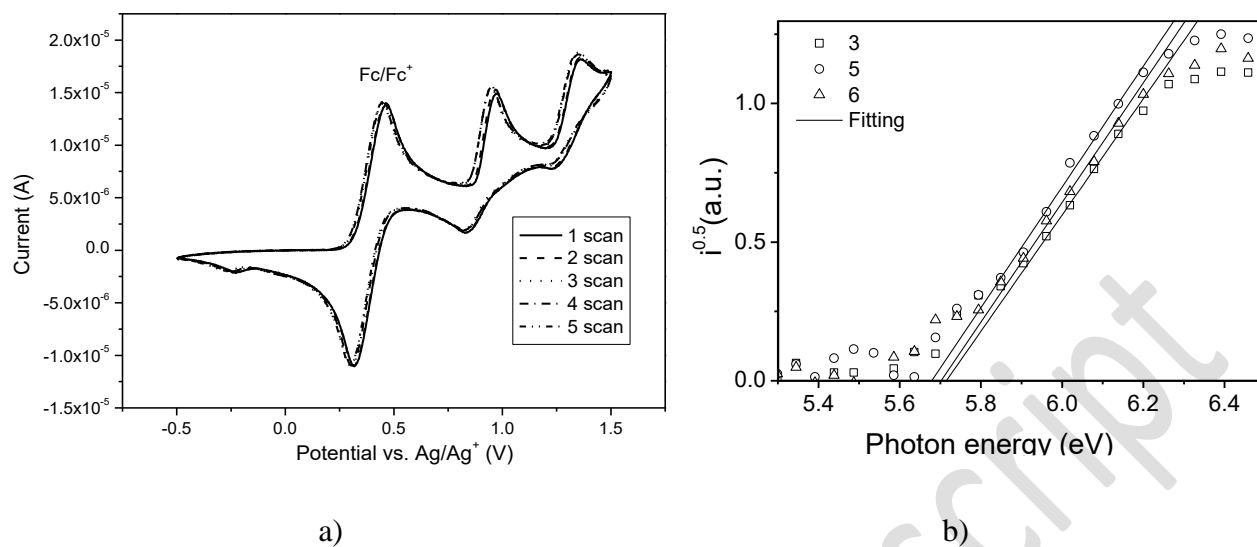


Fig. 3. Cyclic voltammograms of compound **3** (a) and electron photoemission spectra of the thin films of compounds **3**, **5**, **6** (b).

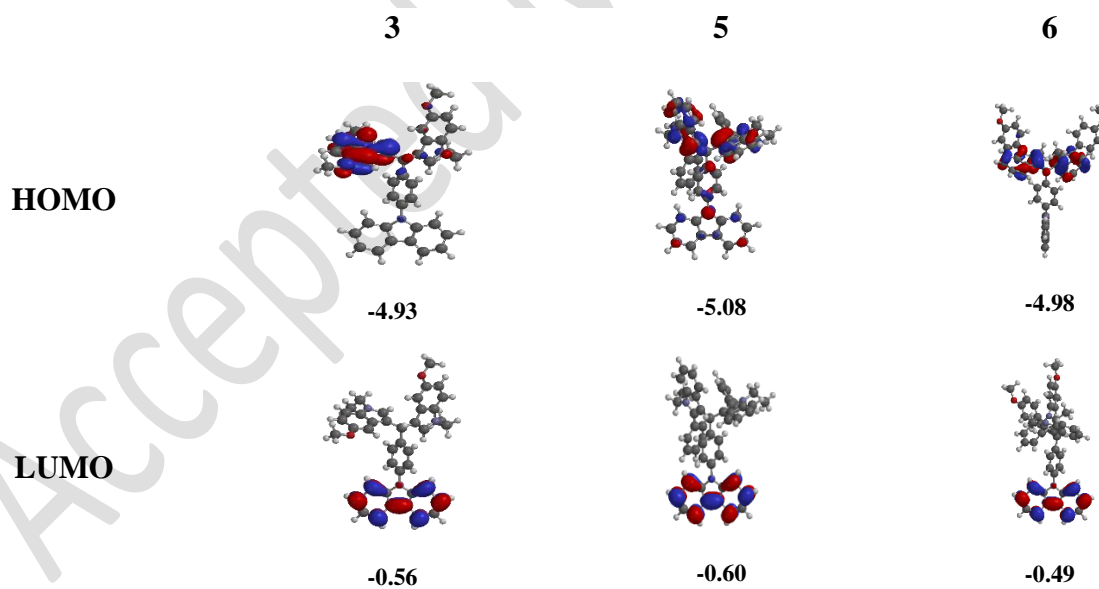


Fig. 4. Electron density distributions and the energy levels of compounds **3**, **5**, and **6** obtained by DFT calculation (B3LYP/6-31G (d, p)).

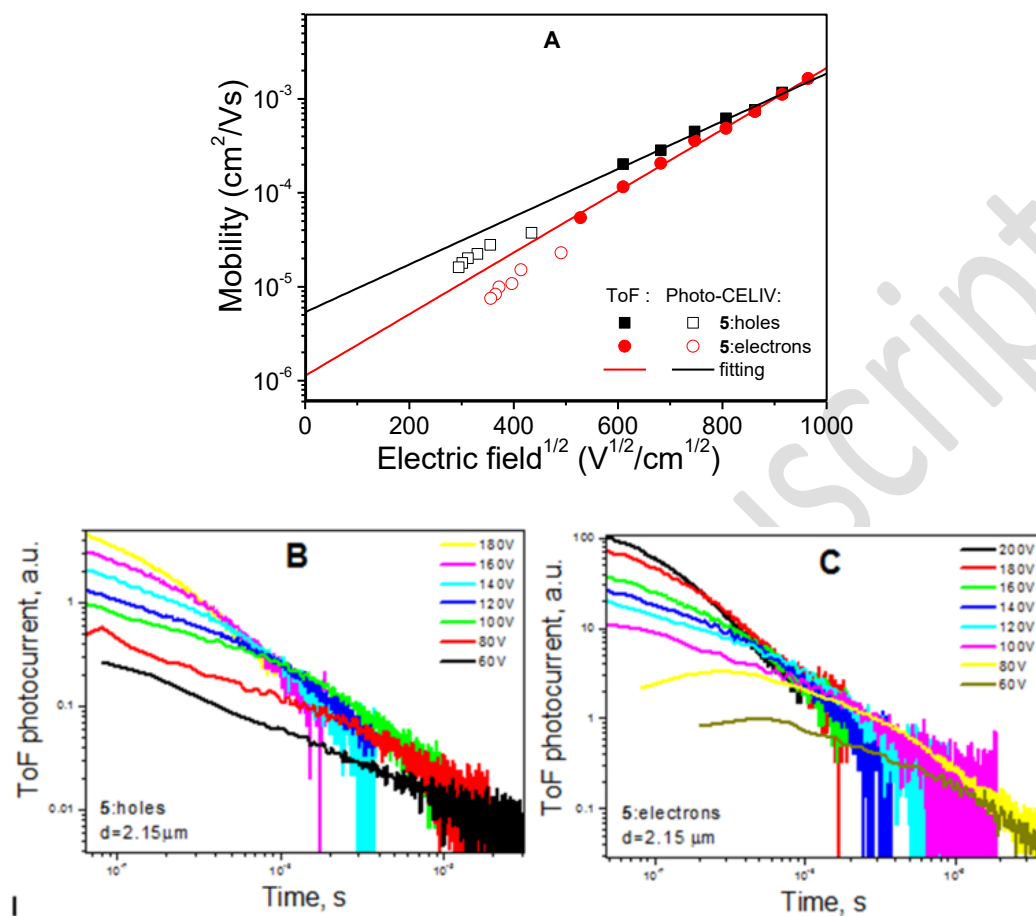


Fig. 5. Hole and electron drift mobility as a function of $E^{1/2}$ for the layer of **5** (A). TOF transient curves in the log-log scales (B, C).

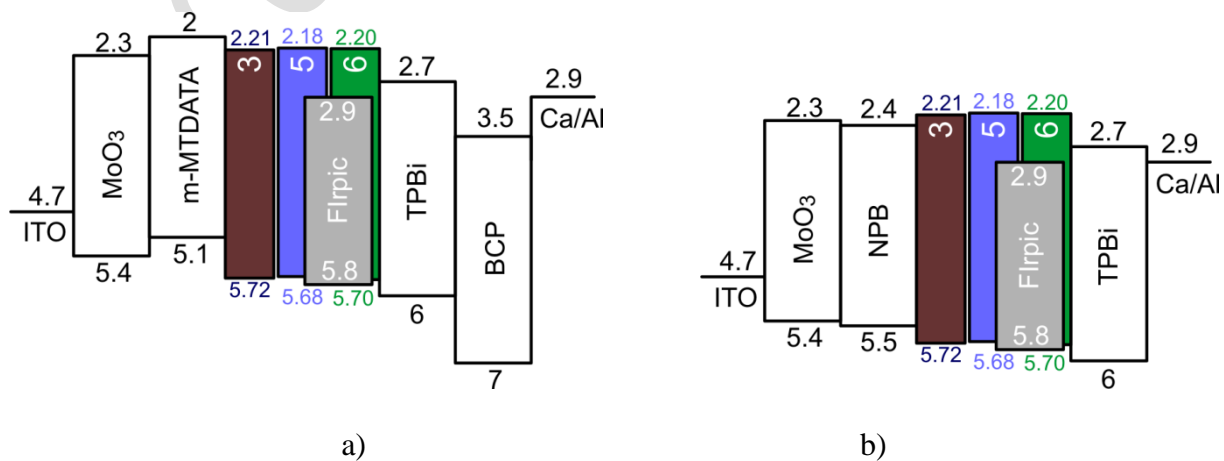


Fig. 6. Energy level diagrams for the devices A, B, C (a) and AI, BI, CI (b).

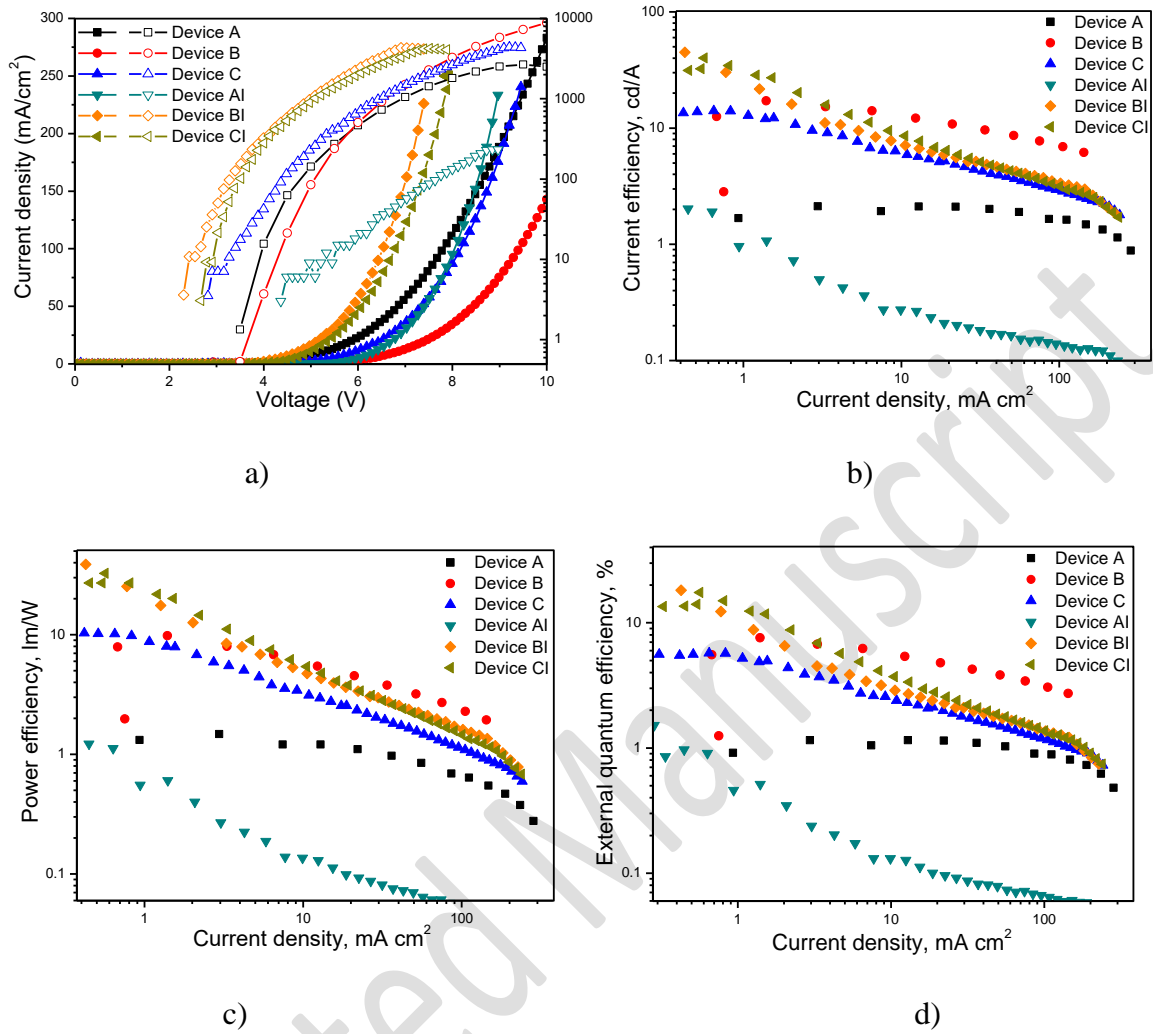


Fig. 7. Current density and brightness versus voltage (a), current (d), power (c), and external quantum (d) efficiencies versus current density dependencies.

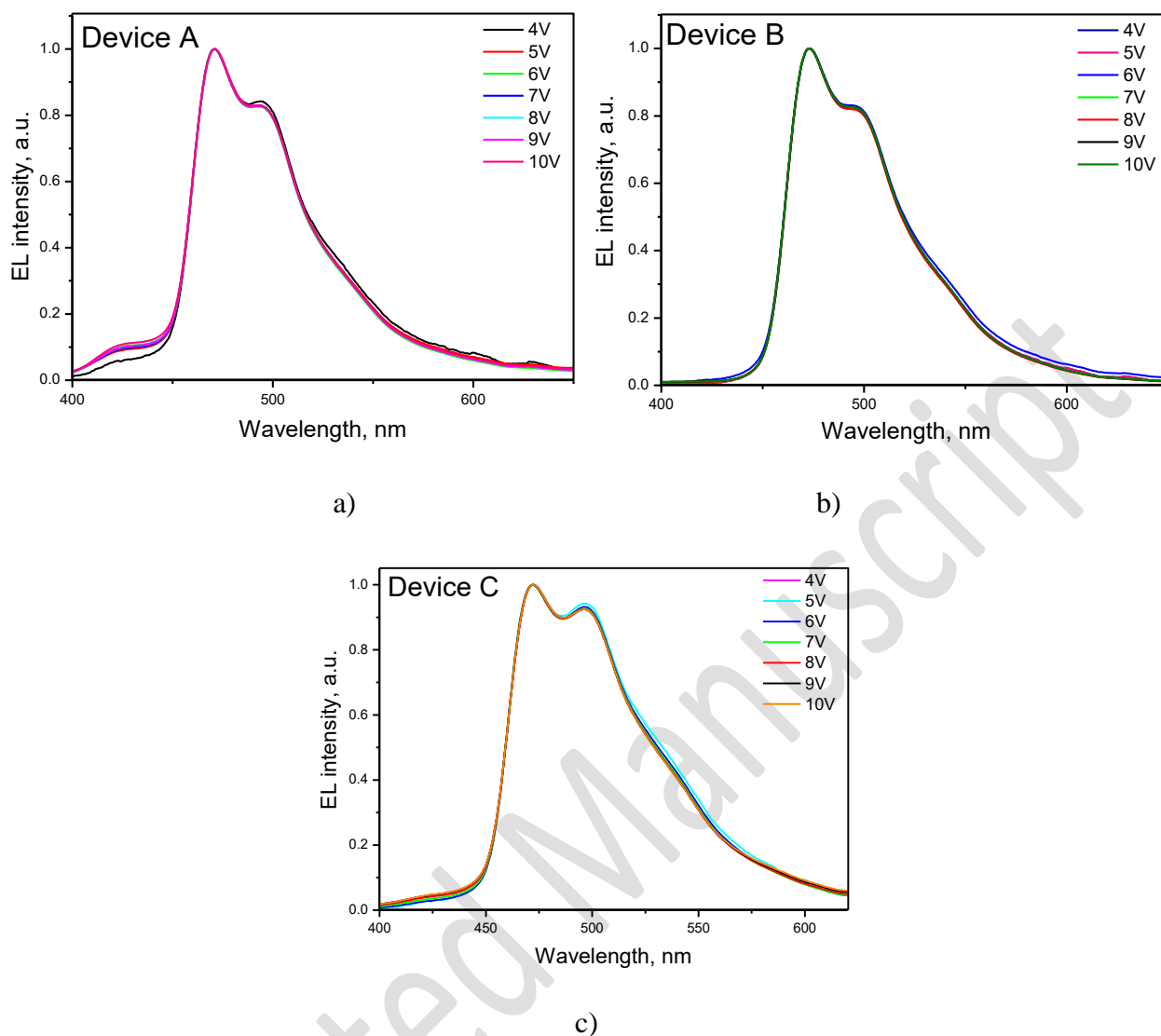


Fig. 8. Electroluminescence spectra of the devices A (a), B (b) and C (c) recorded at the different applied voltages.